CD-ROM INSTRUCTIONS

1. Platforms:
Use computer operating on Windows®2000/XP Professional, Macintosh®10.2, or higher versions, equipped with a CD-ROM drive.

2. Environments:
This CD-ROM has been created in PDF (portable document format), which requires the use of Adobe® Reader®7.0 or higher version. You must install the version of Adobe® Reader® (not included in this CD-ROM) appropriate for your platform.
It also requires the use of an internet browser of Internet Explorer®6.0 or higher version, or Netscape Navigator®7.1 or higher version (both for Windows or Macintosh).

------- Reference -------
Adobe Systems Incorporated
http://www.adobe.com/ → DOWNLOADS → Get Adobe® Reader®

3. Asian Fonts:
Some of the papers included in this CD-ROM have Asian characters (2-byte characters). These characters might not appear properly in some operating systems. For the details, please refer to adobe website.

4. Usage:
- Install Adobe® Reader® in advance.
  For Windows®2000/XP Professional, open the CD-ROM icon within My Computer, then double click "index.html". For Macintosh®, open the CD-ROM icon on the desktop, then double click "index.html".

The 12th International Conference on Electrical Machines and Systems (ICEMS 2009), Tokyo, Japan

ICEMS Tokyo 2009

Proceedings

The 12th International Conference on Electrical Machines and Systems

November 15-18, 2009
Tower Hall Funabori, Tokyo, Japan

DS2G2-5
An EKF for PMSM Sensorless Control Based on Noise Model Identification Using Ant Colony Algorithm
Anbang Wang[1], Qunjing Wang[1], Cungang Hu[1], Zhe Qian[1], Lufeng Ju[1], Jun Liu[2]
[1]*Hefei University of Technology, China,* [2]*Anhui Technical College of Mechanical and Electrical Engineering, China*

DS2G2-6
Simulation of Sensorless Drive for Surface Mounted PM Machine Based on Comprehensive Machine Model
Yi Wang[1], Jianguo Zhu[1], Youguang Guo[1], Shuhong Wang[2], Wei Xu[1], Yongjian Li[1]
[1]*University of Technology, Australia,* [2]*Xi'an Jiaorong University, China*

DS2G2-7
Influences of Rotor Eccentricity on Permanent Magnet Synchronous Motor Characteristics
R. Takahata[1], S. Wakui[1], K. Miyata[1], K. Noma[2], M. Senoo[2]
[1]*Hitachi Ltd., Japan,* [2]*Hitachi Industrial Equipment Systems Co., Japan*

DS2G2-8
Characteristics Measurement of Direct-Drive Brushless DC Motors without Using Dynamometers
C. Y. Wu, M. C. Tasi, S. H. Mao
National Cheng Kung University, Taiwan

DS2G2-9
Load Characteristics Comparisons of Interior Permanent Magnet Synchronous Motors by Pole-Slot Combinations
I. Morita, T. Kanayama, T. Ueta
University of Tokushima, Japan

DS2G2-10
An Improved AC Standstill Inductance Test Method for Interior PM Synchronous Motor Considering Cross-Magnetization Effect
Tao Sun, Soon-O Kwon, Jeong-Jong Lee, Geun-Ho Lee, Jung-Pyo Hong
Hanyang Universisty, Korea

DS2G2-11
Electromagnetic Vibration of Interior Permanent Magnet Brushless Motors under Brushless DC and AC Operation
Haodong Yang[1,2], Zeyin Han[1], Yangsheng Chen[1]
[1]*Zhejiang University, China,* [2]*Changshu Institute of Technology, China*

DS2G2-12
Influence of Design Parameters on Cogging Torque in Directly Driven Permanent Magnet Synchronous Wind Generators
Qiu-ling Deng[1], Shoudao Huang[1], Feng Xiao[2]
[1]*Hunan University, China,* [2]*Hunan Institute of Engineering, China*

Session DS2G3
Induction Machines and Drives (4)

Date: Tuesday, 17 November 2009
Time: 13:30-14:45
Venue: Room G
Chair: Hisao Kubota
Meiji University, Japan

DS2G3-1
Implementation and Verification of the Amplitude Recovery Method Algorithm with the Faults Diagnostic System on Induction Motors
Yukun Liu[1,2], Liwei Guo[1], Chunru Huang[2]
[1]*Hebei University of Science and Technology, China,* [2]*University of Bedfordshire, UK*

DS2G3-2
Three-Level Direct Torque Control Using Novel Phase Compensation Flux Observer
Yaofei Han, Guojun Tan, Xuanqin Wu, Daoming Zhang
China University of Mining and Technology, China

DS2G3-3
Study on Back-to-Back PWM Converter Based on Direct Power Control for Induction Motor Drive
Wanwei Wang, Huajie Yin, Lin Guan
South China University of Technology, China

DS2G3-4
Induction Motor Speed Measurement Using Motor Current Signature Analysis Technique
P. Phumiphak, C. Chat-uthai
King Mongkut's Institute of Technology Ladkrabang, Thailand

DS2G3-5
Steady-State and Transient Characteristics of a Novel *V/f* Controlled Induction Motor
Mineo Tsuji[1], Xiaodan Zhao[1], He Zhang[1], Shin-ichi Hamasaki[1], Shuo Chen[2]
[1]*Nagasaki University, Japan,* [2]*Fuzhou University, China*

DS2G3-6
Characteristics of MRAS Based Induction Motor Sensorless Vector Control System Taking into Account Iron Loss
Mineo Tsuji[1], Fujin Xu[1], Yasutaka Tsuruda[1], Shin-ichi Hamasaki[1], Shuo Chen[2]
[1]*Nagasaki University, Japan,* [2]*Fuzhou University, China*

DS2G3-7
A PWM Strategy for Six-Phase Dual Stator Induction Motor Fed by Two Identical Voltage Source Inverters
Fangbin Cheng, Huan Yang, Rongxiang Zhao, Minglei Zhu
Zhejiang University, China

DS2G3-8
Research of Neuro-Fuzzy-Based Hybrid Efficiency Optimization Control of Inductive Motor
Xie Dongmei
Shenyang Institute of Engineering, China

An Improved AC Standstill Inductance Test Method for Interior PM Synchronous Motor Considering Cross-Magnetization Effect

Tao Sun, Soon-O Kwon, Jeong-Jong Lee, Geun-Ho Lee, Jung-Pyo Hong
Hanyang Univerisity, Seoul, Korea
laplace_sun@hotmail.com, hongjp@hanyang.ac.kr

***Abstract*--An improved AC standstill inductance measurement method for interior permanent magnet synchronous machine (IPMSM) is proposed in this paper. Only the 3-phase voltage source, oscilloscope, and DC voltage source are required, rather than the dynamometer and inverter in the other methods. Depending on the deduced q- and d-axis voltage equations in the stationary reference frame, the q- and d-axis inductances at different current magnetite and vector angle can be calculated by the measured 3-phase voltages and currents. Thus, the saturation and cross-magnetizing effect of the inductances are measurable. This paper will introduce the principle equations, experiment setup, data processing, and results comparison.**

***Index Terms*--Cross-magnetizing effect, Inductance measurement, Interior permanent magnet synchronous motors, and Stationary frame of reference.**

I. Introduction

Interior permanent magnet synchronous motors (IPMSM) have been widely applied in the many fields, due to their high power density, high efficiency and wide operation range characteristics. Because of the permanent magnet, salient structure, and rib on rotor, the inductance of IPMSM becomes especially difficult to calculate and test [1]. A few numerical methods have been proposed to solve the calculation problem [2] [4] [5]. The saturation, cross-magnetizing and other effect can be considered and calculated in these methods. There are also several solutions to measure the inductances [2]-[5]. In [3] an IEEE standard method called AC standstill is introduced. This method applies a single phase AC voltage source to one phase motor winding, and measures the currents and voltages of this phase and another phase in order to calculate the self- and mutual-inductances, and further calculate d- and q-axis inductances with them. It is called standstill because the rotor is locked at each test position. It is obvious that the effect of current vector angle varying cannot be reflected, and hence the cross-magnetizing effect is regardless in this method. Additionally, the flux path in two-phase exciting will be different with the one of three-phase exciting. The other standstill method with considering the both saturation and cross-magnetizing effect is introduced in [4]. It fixes the rotor position and uses a vector controller to generate a stepwise d- or q-axis voltage, meanwhile, keep the other axis current constant. According to the current response, the two-axis inductances can be calculated. The difficulty of this method is the generation of the stepwise d- or q-axis voltage. In the ordinary 3-phase inverter, it cannot be directly obtained from the pulse width modulation (PWM) voltage. A high precision low-pass filter must be used. According to phase shift between the flux linkages under the load condition and no-load condition in the steady state, authors of [5] measured the dq-axis inductances in the operation conditions. In this method, for the desired current magnitude and vector angle, keep the d-axis current and adjust the load torque so that the q-axis current can be controlled to the desired value. A dynamometer is required to apply an adjustable load torque to the test motor. A power meter is used to measure the power factor and then calculate the current vector angle. Moreover, the vector-control motor drive, and low-pass filter, etc. are also necessary. Therefore, the system setup becomes complicated and relative expensive.

The methods in [4] and [5] can measure the inductance with considering the cross-magnetizing and saturation effects. When the proper motor drive is absent, however, these inductance test methods become unavailable. In addition, the utilization of dynamometer in [5] will increase the cost of the experiment system. Considering the practical requirements, this paper proposes a simple method to measure the d- and q-axis inductance of IPMSM. It is based on the AC standstill method, i.e. processed in standstill condition so that the dynamometer and other load equipments are not necessary. It uses a 3-phase AC voltage source so that the vector control drive is not required. It only measures the phase currents and phase voltages, so the power meter is eliminated. Hence, it is very suitable for normal laboratory experiment. The most meaningful point is that this method also can consider the saturation and cross-magnetizing effect. In this paper, the principle of this method will be introduced. And then, based on the deductive equations, the experiment scheme and the processing methods of measured data will be proposed. After briefly introduce the inductance calculation method used in this paper, both a concentrated-winding IPMSM and a distributed-winding IPMSM will be tested and compared with the corresponding calculated results.

II. Improved AC Standstill Test Method

In the standstill condition, all measured variables are in the stationary frame of reference. However, the desired d- and q-axis inductances are the variables of the synchronous frame of reference. It is necessary to find the relationship between the measured variables and desired

inductances.

A. Inductance in Stationary Frame of Reference

The voltage equation of the IPMSM in the stationary frame of reference is described in (1) [6].

$$\begin{bmatrix} v_q^s \\ v_d^s \end{bmatrix} = \begin{bmatrix} r_s & 0 \\ 0 & r_s \end{bmatrix} \begin{bmatrix} i_q^s \\ i_d^s \end{bmatrix} + \begin{bmatrix} p & 0 \\ 0 & p \end{bmatrix} \begin{bmatrix} \lambda_q^s \\ \lambda_d^s \end{bmatrix}$$

$$\begin{bmatrix} \lambda_q^s \\ \lambda_d^s \end{bmatrix} = \begin{bmatrix} L_q^s & -L_{qd}^s \\ -L_{qd}^s & L_d^s \end{bmatrix} \begin{bmatrix} i_q^s \\ i_d^s \end{bmatrix} + \begin{bmatrix} \lambda_m \sin\theta_{er}^s \\ \lambda_m \cos\theta_{er}^s \end{bmatrix}$$

$$\begin{aligned} L_q^s &= L + \Delta L\cos(2\theta_{er}^s) \\ L_d^s &= L - \Delta L\cos(2\theta_{er}^s) \\ L_{qd}^s &= \Delta L\sin(2\theta_{er}^s) \end{aligned} \tag{1}$$

where r_s is the phase resistance, λ_m is the flux linkage of PM, p represents the d/dt operator, the subscript e represents the unit in electrical angle, θ_{er}^s is the rotor position in stationary frame of reference, and the L and ΔL are calculated by (2).

$$\begin{aligned} L &= \frac{L_q^r + L_d^r}{2} \\ \Delta L &= \frac{L_q^r - L_d^r}{2} \end{aligned} \tag{2}$$

i.e.,

$$\begin{aligned} L_q^r &= L + \Delta L \\ L_d^r &= L - \Delta L \end{aligned} \tag{3}$$

where L_q^r and L_d^r are the desired q- and d-axis inductances in the synchronous frame of reference.

B. Equations of Measurement Method

(1) also can be expressed as (4),

$$\begin{aligned} v_q^s &= r_s i_q^s + \left(L + \Delta L\cos(2\theta_{er}^s)\right)\frac{d}{dt}i_q^s - 2\omega_{er}^s \Delta L\sin(2v) i_q^s \\ &\quad - \Delta L\sin(2\theta_{er}^s)\frac{d}{dt}i_d^s - 2\omega_{er}^s \Delta L\cos(2\theta_{er}^s) i_d^s + \omega_{er}^s \lambda_m \cos\theta_{er}^s \\ v_d^s &= r_s i_d^s + \left(L - \Delta L\cos(2\theta_{er}^s)\right)\frac{d}{dt}i_d^s + 2\omega_{er}^s \Delta L\sin(2\theta_{er}^s) i_d^s \\ &\quad - \Delta L\sin(2\theta_{er}^s)\frac{d}{dt}i_q^s - 2\omega_{er}^s \Delta L\cos(2\theta_{er}^s) i_q^s - \omega_{er}^s \lambda_m \sin\theta_{er}^s \end{aligned} \tag{4}$$

It is evident that the terms with ω_{er}^s can be eliminated in the standstill condition. And in order to eliminate the sine and cosine terms, the rotor position θ_{er}^s is set to 0°. Thus the equations are simplified as (5).

$$\begin{aligned} v_q^s &= r_s i_q^s + L_q^r \frac{d}{dt} i_q^s \\ v_d^s &= r_s i_d^s + L_d^r \frac{d}{dt} i_d^s \end{aligned} \tag{5}$$

where the v_q^s, v_d^s, i_q^s and i_d^s are the q- and d-axis voltages and currents. According to the Clarke's transformation in the stationary frame of reference (6), they can be represented by 3-phase voltages and currents that are directly measurable variables. In practice, (5) is modified as (7) in order to satisfy the digital measurement equipment.

$$\begin{bmatrix} f_q^s \\ f_d^s \end{bmatrix} = \frac{2}{3}\begin{bmatrix} 1 & -\frac{1}{2} & -\frac{1}{2} \\ 0 & -\frac{\sqrt{3}}{2} & \frac{\sqrt{3}}{2} \end{bmatrix} \begin{bmatrix} f_a^s \\ f_b^s \\ f_c^s \end{bmatrix} \tag{6}$$

$$\begin{aligned} \left[2v_a(k) - v_b(k) - v_c(k)\right] &= r_s\left[2i_a(k) - i_b(k) - i_c(k)\right] \\ &\quad + L_q^r \frac{\left[2i_a(k) - i_b(k) - i_c(k)\right] - \left[2i_a(k-1) - i_b(k-1) - i_c(k-1)\right]}{T_s} \\ \left[v_c(k) - v_b(k)\right] &= r_s\left[i_c(k) - i_b(k)\right] \\ &\quad + L_d^r \frac{\left[i_c(k) - i_b(k)\right] - \left[i_c(k-1) - i_b(k-1)\right]}{T_s} \end{aligned} \tag{7}$$

where f represents the voltage or current variable, k means the k[th] value of data, and T_s is the sampling time of the measurement equipment. Finally, in order to express the relationship between the inductances and current vector, the 3-phase current should be transformed to the magnitude and angle of the vector in the synchronous frame of reference (8), (9) and (10)

$$\begin{bmatrix} i_q^r \\ i_d^r \end{bmatrix} = \frac{2}{3}\begin{bmatrix} \cos\theta_{er}^s & \cos(\theta_{er}^s - \frac{2\pi}{3}) & \cos(\theta_{er}^s + \frac{2\pi}{3}) \\ \sin\theta_{er}^s & \sin(\theta_{er}^s - \frac{2\pi}{3}) & \sin(\theta_{er}^s + \frac{2\pi}{3}) \end{bmatrix} \begin{bmatrix} i_a^s \\ i_b^s \\ i_c^s \end{bmatrix} \tag{8}$$

$$I_a = \sqrt{(i_q^r)^2 + (i_d^r)^2} \tag{9}$$

$$\beta = -\arctan\left(\frac{i_d^r}{i_q^r}\right) \tag{10}$$

where θ_{er}^s is 0° as assumed before, I_a is the magnitude of current vector, and β is the angle of current vector referred to q-axis.

III. Experiment Devices and Setup

A. Experiment Scheme and Devices

The main purpose of this paper's method is to measure the d- and q-axis inductances considering the saturation and cross-magnetizing effect, and with relatively normal laboratory equipments and simple system. According to the deductive equations, the ideal 3-phase AC voltage source (or current source) is required. In this paper, however, the voltage source will be applied. In the standstill state, there is no back electromotive force

(Back-EMF) in each phase. The rated phase current usually can be reached at very low voltage exciting. Therefore, the low voltage range has priority when select the voltage source, in order to increase the input signal precision. In addition, there are current components in the equivalent iron-loss resistances [5], which are not the torque-producing component and rises as the source frequency increasing. Thus relatively low frequency of the AC source also is suggested.

As described in (7), totally there are six variables that should be measured. Unfortunately, more measure channels in oscilloscope implies more expensive price. Due to the asymmetric spatial distribution of phase inductance, for the Wye-connection winding, the sum of the 3-phase voltages is no longer zero. Meanwhile, the sum of 3-phase currents always equals to zero. Thus, 3-phase voltage and 2-phase current should be measured. In the case of this paper, a 4-channel oscilloscope is applied. One among the 4 channels is used to measure the phase c voltage and phase b current, and combine the two groups of measured data in later manufacture.

In order to find the rotor zero position, a DC voltage generator is used. According to the inverse Clarke's transformation, a d-axis current can be generated by exciting series phase b and c with a DC voltage as shown in (11).

$$\begin{bmatrix} i_a^s \\ i_b^s \\ i_c^s \end{bmatrix} = \begin{bmatrix} 1 & 0 \\ -1/2 & -\sqrt{3}/2 \\ -1/2 & \sqrt{3}/2 \end{bmatrix} \begin{bmatrix} 0 \\ i_d^s \end{bmatrix} = \begin{bmatrix} 0 \\ -i_d^s\sqrt{3}/2 \\ i_d^s\sqrt{3}/2 \end{bmatrix} \tag{11}$$

This d-axis current will align the permanent magnet of one pole with the d-axis. After aligning the zero position, the rotor may be fixed by a vice grid pliers or a brake. Due to the rotation of current vector, it is not necessary to rotate the rotor at each position. The experiment Scheme applied in this paper is shown in Fig. 1 (a), while the practice experiment setup is shown in Fig. 2. The total experiment devices include a 50-Hz 3-phase AC source, a 4-channel oscilloscope, a vice grid pliers, and a DC voltage generator. If the proper 3-phase AC voltage source is unavailable, a 3-phase PM synchronous motor with low total harmonic distortion Back-EMF could be used to generate the nearly ideal 3-phase voltage as shown in Fig. 1 (b). In the case of large Back-EMF, the rheostat can be used to reduce the amplitude of the input voltages. And it is better to use the DC voltage generator to drive the traction DC motor rather than a voltage-chopping controller, in order to generate constant frequency.

B. Experiment IPMSM Models

Two IPMSMs with concentrated winding and distributed winding are analyzed and tested in this paper in order to verify the applicability of the proposed method. These two motors are designed for high speed operation. The rated speed reaches 26000rpm. It is difficult to find a proper drive to test this kind of high speed motor during the proto design. However, the test results will be quite incorrect in the low speed operation condition due to the influence of the losses components. Therefore, the standstill test method becomes more meaningful. The cross-sections of these two motors are shown in Fig. 3 (a) and (b), respectively. And their specifications are listed and compared in Table I.

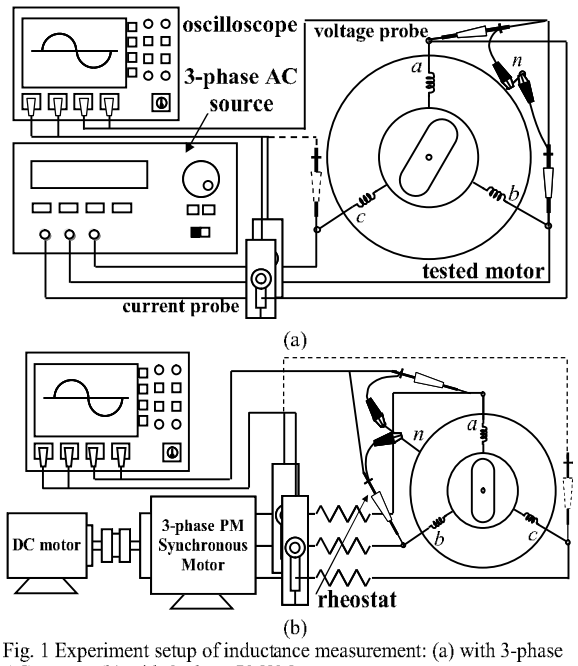

Fig. 1 Experiment setup of inductance measurement: (a) with 3-phase AC source; (b) with 3-phase PMSM

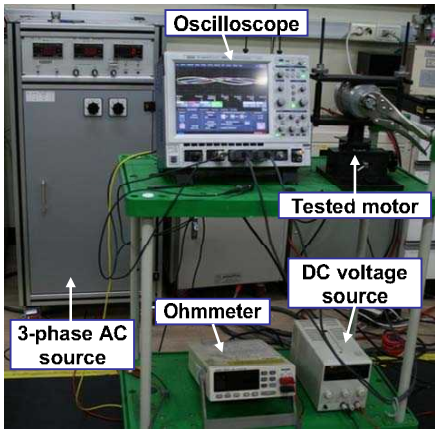

Fig. 2 Experiment setting of inductance measurement in this paper

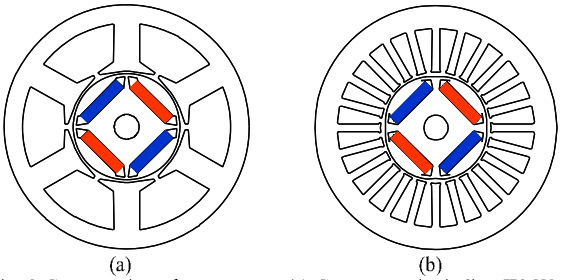

Fig. 3 Cross-section of test motors: (a) Concentrated winding IPMSM; (b) Distributed winding IPMSM

TABLE I
SPECIFICATION OF TWO ANALYZED IPMSMS

Parameters	Value		Unit
	Contributed winding	Distributed winding	
Stator outer radii/ Rotor outer radii	80 / 34.5		mm
Airgap length/ Stack length	0.8 / 35		mm
Volume of PM	16×3.5×34		mm^3
Material of core	cogent		
No. of turns in series connected	58	52	turn
No. of parallel circuits	2		
Phase resistance (@20ºC)	0.159	0.145	Ohm
Rated current	8.8		A_{rms}

IV. EXPERIMENT DATA AND PROCESSING

A. Experiment Results

In the proposed method, the waveforms of the currents and voltages of the concentrated winding IPMSM measured by digital oscilloscope is shown in Fig. 4. Because of the different phase inductance in the certain position, it can be seen that the magnitude of the each phase voltage or current is different to the others. These test results are stored as ASCII format data so that the computer program can handle them.

B. FFT Filter for Smoothing Measured Data

The waveforms in Fig. 4 are measured and saved with a digital oscilloscope. The measured voltages and currents hence are discrete-time data. It is obvious that there is much noise in the measured wave forms so that the data cannot be used directly. By means of the Fast Fourier Transform (FFT) filter, the Fourier components whose frequencies are higher than the frequency in (12) can be removed from the original experiment data.

$$f_{threshold} = \frac{1}{n\Delta T} \tag{12}$$

where n is the number of data points considered at one time, and ΔT is the abscissa spacing between two adjacent data points. Fig. 5 shows the comparison between the original data and filtered wave form of phase a voltage.

C. Ripple Elimination

Fig. 6 shows the calculated inductance according to the measured phase voltages and currents and deductive formula (7). It can be seen that the raw inductance results have serious ripples. The main reason is that the slots and teeth of stator produce the different permeability in the spatial distribution. Additionally, due to the asymmetric circuit, the variation of current magnitude and vector angle also may generate different saturation and cross-magnetizing effect. In order to eliminate the ripple of calculated inductances, the Polynomial Least-square function is applied to fit the inductance curve in this

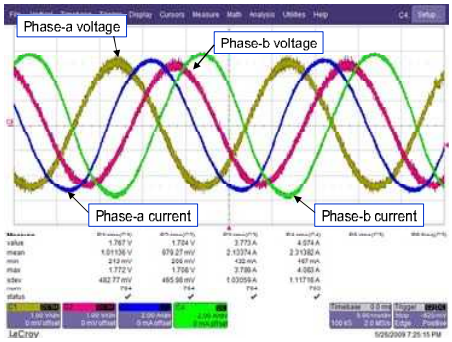

Fig. 4 Measured phase voltages and currents of the concentrated winding IPMSM at about 3 A_{rms}.

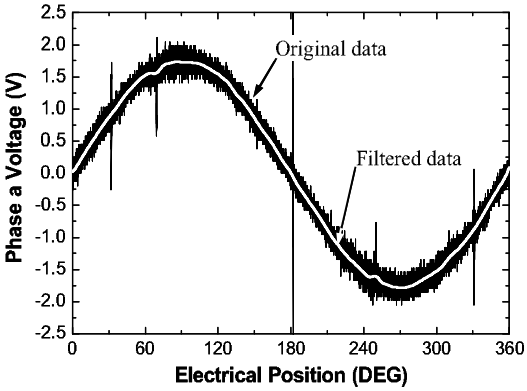

Fig. 5 Comparison of the original data and the filtered data of phase-a voltage waveforms.

paper. A general M-1 orders polynomial least-square function is described in (13).

$$f(x) = a_0 + a_1 x + a_2 x^2 + \ldots + a_M x^{M-1} \tag{13}$$

where a_0, a_1, $a_2 \ldots a_{M-1}$ are chosen to minimize the least-square loss function (14). [7]

$$\chi^2 = \sum_{i=1}^{N} \left[\frac{y_i - \sum_{k=1}^{M} a_k X_k(x_i)}{\sigma_i} \right]^2 \tag{14}$$

where σ_i is the measurement error of the i^{th} data, and N is the number of sampling data. According to the relationship of current vector angle and electrical position as shown in Fig. 7, the data from 60º to 240º electrical position can cover the current vector angle from the -90º to 90º. Thus, the data in this section is selected and processed by curve fitting. The fitting results of concentrated winding IPMSM and distributed winding IPMSM are shown in Fig. 8 (a) and (b), respectively.

V. CALCULATION METHOD

The inductance calculation method used in this paper is introduced in [7]. A phasor diagram of IPMSM is shown in Fig. 9. In the solid-line part, it can be seen that there are the relationships (15) and (16)

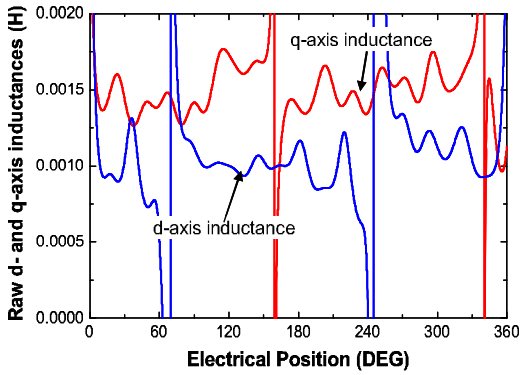

(a)

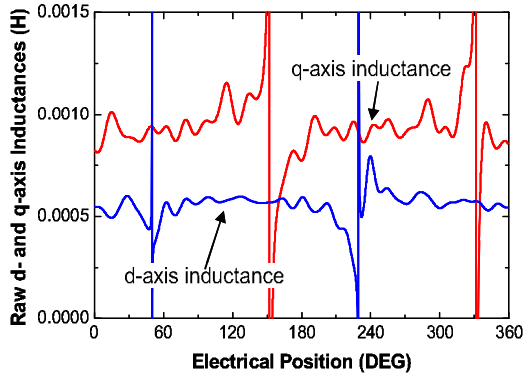

(b)

Fig. 6 Raw measured d- and q-axis inductances at certain voltage: (a) concentrated winding IPMSM; (b) distributed winding IPMSM

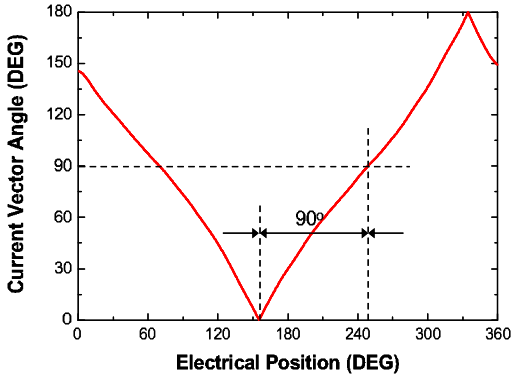

Fig. 7 Relationship between current vector angle and electric position (e.g. concentrated winding IPMSM)

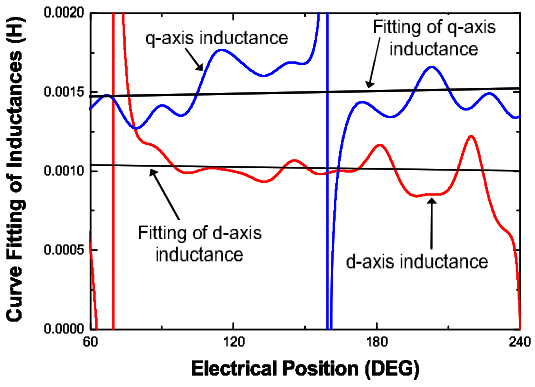

(a)

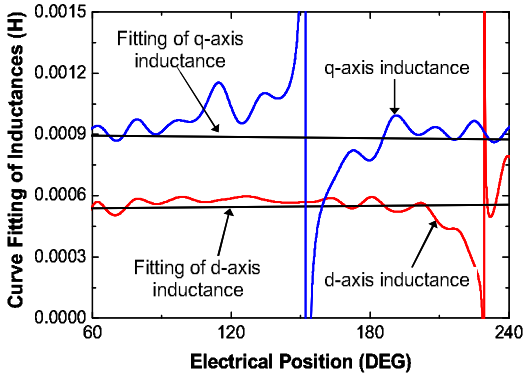

(b)

Fig. 8 Curve fitting of raw inductance results: (a) concentrated winding IPMSM; (b) distributed winding IPMSM.

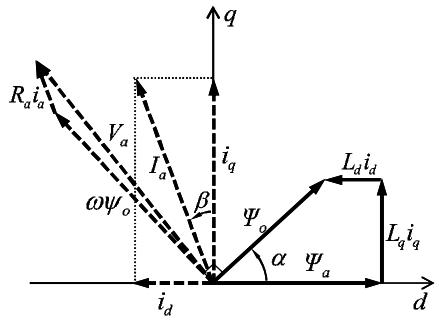

Fig. 9 Phasor diagram of IPMSM

$$L_d = \frac{\psi_0 \cos\alpha - \psi_a}{i_d} \tag{15}$$

$$L_q = \frac{\psi_0 \sin\alpha}{i_q} \tag{16}$$

where ψ_a is the flux linkage generated by permanent

VI. Comparisons of Results and Discussion

The d- and q-axis inductances of the concentrated winding IPMSM and distributed winding IPMSM calculated by the above method are shown in Fig. 10 (a) and (b), respectively. It can be seen that the inductances of distributed winding IPMSM have no much differences as the current magnitude and vector angle varying, which means the significant cross-magnetizing and saturation effects can not be reflected well. Due to the air cooling method, the current can not reach high. Therefore, the motor always operates under the unsaturated condition.

The d- and q-axis inductances of these two motors measured with the proposed method are shown in Fig. 11 (a) and (b), respectively. Compared with the calculated results, the experimental are very similar to them. It can be seen that the measured d-axis inductances are larger than those of calculation. This is because the rotor d-axis is almost aligned with the stator tooth when find the motor 0° electrical position and without eliminating the space harmonics. The measured inductances of concentrated winding IPMSM have relatively greater differences with the calculated. As mentioned before, the

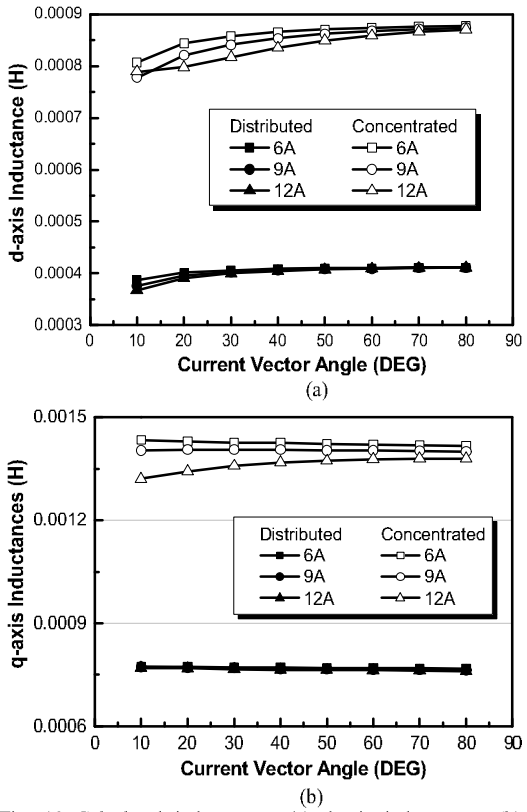

Fig. 10 Calculated inductances: (a) d-axis inductances; (b) q-axis inductances

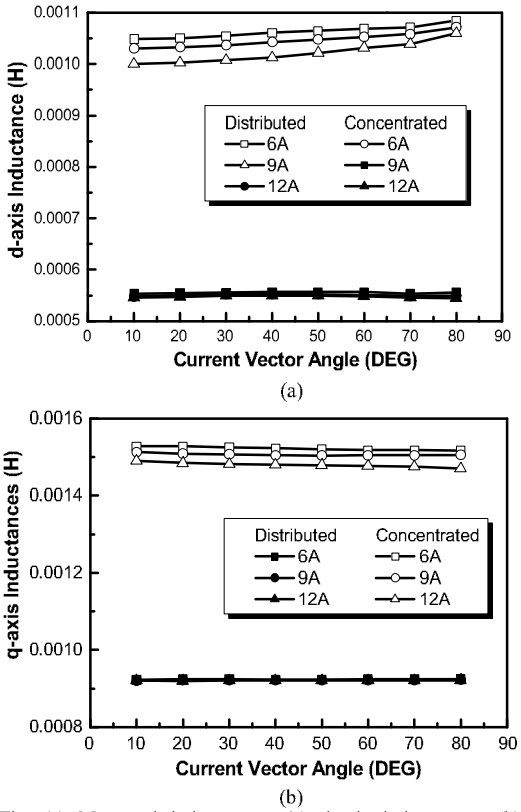

Fig. 11 Measured inductances: (a) d-axis inductances; (b) q-axis inductances

deductive equations are based on the sinusoidal winding distribution. The concentrated winding generates more space harmonics which strongly influence the accuracy of the principle equations. Additionally, the analysis process does not consider the current components in the iron-loss equivalent resistances. Therefore, larger current is used to produce the flux linkage in the numerical calculation process.

Due to the sinusoidal current wave form, the denominator current terms in (7) may generate the singularity points in the entire electrical period. The measured inductances around these singularity points are strongly distorted, which restricts the measurable inductance range. Hence, it can be seen that there is bullish trend near the 80^{o} in the tested d-axis inductance. However, the simplicity and acceptable accuracy make this method be a prefer choice in some situation.

VII. Conclusion

The inherent drawback or complicated system configuration lead the existed IPMSM inductance test methods are not always available. Based on the conventional AC standstill method, this paper proposed a relatively simple experiment method to measure the d- and q-axis inductance of IPMSM in the stationary reference frame. By using the measured 3-phase AC voltages and currents, FFT smoothing and least-square curve fitting, the d- and q-axis inductances reflecting cross-magnetizing and saturation effects can be obtained. Compared with the calculated results, the inductances measured in this method are reliable, especially for the distributed winding motor..

References

[1] R. Dutta, and M. F. Rahman, "A comparative analysis of two test methods of measuring d- and q-axis inductances of interior permanent magnet machine," *IEEE Trans. Magn.*, Vol. 42, No. 11, Nov. 2006.

[2] T. Sun, S. O. Kwon, J. P. Hong, etc., "Investigation and Comparison of Inductance Calculation Methods in Interior Permanent Magnet Synchronous Motors," *Proc. of 11th Int. Conf. on Electrical Machines and Systems (ICEMS 2008)*, Wuhan (China), Oct. 2008, pp. 3131-31368.

[3] *IEEE Standard Procedure for Obtaining Synchronous Machine Parameters by Standstill Frequency Response Testing*, IEEE Standard 115A-1987, 1987

[4] B. Stumberger, G. Stumberger, etc., "Evaluation of saturation and cross-magnetization effects in interior permanent-magnet synchronous motor," *IEEE Trans. Ind. Appl.*, Vol. 39, No. 5, Sept./Oct. 2003.

[5] K. M. Rahman and S. Hiti, "Identification of machine parameters of a synchronous motor," *IEEE Trans. Ind. Appl., Vol. 41, No. 2, Mar./Apr. 2005.*

[6] G.D. Andreescu, etc., "Combined Flux Observer With Signal Injection Enhancement for Wide Speed Range Sensorless Direct Torque Control of IPMSM Drives," *IEEE Trans. Energy Conv.*, vol.23. no. 2,pp.393-402, June. 2008.

[7] W. H. Press, etc., *Numerical Recipes in C: The Art of Scientific Computing.* Cambridge University Press, Oct. 1992.